

Received November 20, 2017, accepted December 23, 2017, date of publication December 28, 2017, date of current version February 28, 2018.

Digital Object Identifier 10.1109/ACCESS.2017.2787801

Ranging Method for Navigation Based on High-Speed Frequency-Hopping Signal

EN YUAN[✉], WANGDONG QI, (Member, IEEE), PENG LIU[✉], LI WEI, AND LONGLIANG CHEN

Department of Network Engineering, Army Engineering University, Nanjing 210007, China

Corresponding author: Wangdong Qi (wangdongqi@gmail.com)

This work was supported by the National Natural Science Foundation of China under Grant 61273047, Grant 61402520, and Grant 61573376.

ABSTRACT The lack of sufficient spectral resources in many alternative positioning, navigation, and timing (APNT) systems for aviation has led to the problem of mutual interferences. Building APNT system with the cognitive radio and frequency-hopping (FH) techniques can resolve above problem, however, the main challenge is to achieve a long and high-precision range with high-speed FH signals. In this paper, we propose a novel ranging method called time–frequency matrix ranging (TFMR), which is based on the FH signals. Using the TFMR method, we built a jam-resistant APNT system to meet the accuracy and coverage requirements of aviation. We employed a dual-tone signal for the TFMR to estimate the pseudorange between the ground stations and the aircrafts. One major challenge we faced was that what was good for ranging accuracy was bad for coverage. For example, increasing the dual-tone interval can improve the ranging accuracy; however, this led to a decrease in the unambiguous measurement range (UMR). To overcome this challenge, we employed different dual-tone intervals in different hops of the frequency-hopping signal. Finally, we formed a time–frequency matrix, so that a high UMR could be guaranteed without any harmful consequences on the ranging accuracy in the middle to high levels of the signal-to-noise ratio. The Cramér–Rao lower bound of TFMR is derived as the benchmark of the method. Using extensive simulations, we investigated the ranging performance of the TFMR method. The simulation results showed that the proposed TFMR could satisfy the APNT requirements of the Federal Aviation Administration.

INDEX TERMS Navigation, frequency hopping, pseudorange.

I. INTRODUCTION

The Global Navigation Satellite System (GNSS) is an important part of the aviation infrastructure because it provides global positioning, navigation, and timing (PNT) services. If the GNSS in the aviation sector fails, it may give rise to serious security-related accidents.

However, the GNSS signal is weak and susceptible to interference [1]. In recent years, a number of security problems have been recorded with the Global Positioning System (GPS), which is the most widely used GNSS. On 4 December 2011, an American Lockheed Martin RQ-170 Sentinel unmanned aerial vehicle was captured by Iranian forces by using jamming and cheating maneuvers. In May 2012, the GPSs of over 500 aircrafts flying over South Korea's Incheon and Gimpo airports stopped working because of GPS jammers used by North Korea. This kind of intentional large-scale jamming of GPSs will have an immense negative impact on the aviation system.

Therefore, it is necessary to develop alternative positioning, navigation, and timing (APNT) systems for aviation so that jam-resistant PNT services are provided when the GNSS fails. The United States Federal Aviation Administration (FAA) proposed three APNT systems, including DME/DME networks constructed by distance measuring equipment (DME), passive wide area multilateration (P-WAM), and pseudolites (PLs) [2]. The German Aerospace Center proposed another APNT system called the L-band Digital Aeronautical Communication System 1 (LDACS1) [3]. Further studies about these APNT systems are presented in [4]–[11]. These APNT systems are based on existing systems and can be constructed quickly from these existing systems.

However, these APNT systems operate at fixed frequencies, and their spectra overlap, which causes mutual interference. For example, the spectrum for the DME ranges from 960 to 1215 MHz, and it is divided into 252 channels;

a fixed channel is assigned to each ground transponder. LDACS1 works in the lower part of the L-band (960–1164 MHz), and this band overlaps with that of the DME. We investigated the interference between DME and LDACS1, and the results indicated the existence of serious mutual interference between the two systems [12]. Besides, there were other systems that worked in the same frequency band, such as GPS L5 and the Joint Tactical Information Distribution System (JTIDS) [4].

It is difficult to avoid the overlapping of spectra between systems because of the lack of spectral resources; however, some unused discontinuous spectra still remain. The operating frequency of a ground transponder is fixed, and it has a bandwidth of only 1 MHz. Therefore, even when multiple DME ground transponders are used in a region, some unused discontinuous channels are still present on the spectrum. However, the unused discontinuous spectrum is different in different regions. As the location of the aircraft changes rapidly, the spectrum to be used by the aircraft also changes rapidly.

The cognitive frequency-hopping (FH) technique can be used effectively in this situation because it combines the cognitive radio and FH techniques. The cognitive radio technique can sense a spectrum to obtain an unused discontinuous spectrum in real time. The FH technique can effectively use a discontinuous spectrum over a wide frequency band to obtain substantial anti-jamming gain control. Therefore, the cognitive FH technique can dynamically adjust FH patterns according to the spectrum utilization; this technique can be applied to wireless communications [13]–[17]. For example, the cognitive FH technique is used in aircraft communication to increase the resource utilization and enhance the anti-jamming ability [15]. And carefully design the frequency hopping sequence can improve the anti-jamming ability of the cognitive FH system [16]. It is possible to apply the cognitive FH technique to aviation navigation and build a new APNT system with high anti-jamming ability. Spectrum-sensing algorithm in communication can be used in aviation navigation. Real-time communication is possible between the aircraft and the ground stations (GSs); therefore, the spectrum-sensing results can be transmitted in real time. Based on this information, the spectrum-management algorithm and the spectrum-sharing algorithm in communication can also be applied to aviation navigation.

To build such APNT systems, a number of problems need to be resolved. However, the main challenge is to achieve a long and high-precision range with high-speed FH signals. APNT needs to provide navigation, which requires hundreds of kilometers of range. The FAA has different positioning accuracy requirements for various operations of the APNT system. For example, for lateral navigation, the FAA requires positioning accuracy better than 0.3 nm (nautical miles) 95% of the time, and for surveillance, it requires 92.8 m of positioning accuracy 95% of the time [5]. Therefore, the challenges faced are as follows:

- 1) The ranging methods are limited because of the short resident time and limited instantaneous bandwidths of high-speed FH signals.
- 2) The signal received by the aircraft undergoes a Doppler shift because of the high speed of the aircraft.

In this study, we propose a ranging method for aviation navigation based on high-speed FH signals; we have called this the time-frequency matrix ranging (TFMR) method. Two major highlights of the proposed TFMR method are as follows:

- 1) Based on the high-speed FH signal, we propose a passive ranging method. Time-synchronized GSs transmit different dual tones in different hops of the FH signal. By measuring the phase difference of a dual-tone signal and combining the multi-hop signal to construct a time-frequency matrix (TFM), the aircraft estimates the pseudorange to the GS. By making a phase difference of dual tone, the influence of the initial carrier phase on the ranging was eliminated, and the influence of the short resident time of the high FH signal on the unambiguous measurement range (UMR) [18] was overcome by using TFM. The proposed TFMR can achieve high accuracy across a large area.
- 2) The TFMR method uses prior-knowledge-based frequency estimation. According to the prior knowledge about the transmitted dual-tone signal, the frequency offset of each hop is estimated to reduce the Doppler shift and the inaccuracy of the carrier frequency to the estimated pseudorange. The proposed TFMR can effectively improve the ranging accuracy more than the independent estimation method that estimates the frequency of each tone independently.

The rest of the paper is organized as follows. In Section II, the system model for the aviation navigation scenario is described. The ranging method based on the dual-tone signal is introduced in Section III, and the tradeoff between the ranging accuracy and the UMR is also analyzed in this section. Then, we propose a TFMR method based on the FH signal in Section III. In Section IV, we present a pseudorange estimation method for the TFMR. And the Cramer-Rao lower bound (CRLB) of the range estimation is derived in Section V. Our simulation results are analyzed in Section VI. The conclusions are drawn in Section VII.

II. SYSTEM MODEL

A. BASIC MODEL

Consider a typical APNT system deployment scenario in which we need to position many aircrafts by several GSs with known positions, as shown in Fig. 1. The GSs transmit FH signal in the time division mode, and the aircrafts receive the FH signal and calculate their own positions. The antenna of the GS is very far from the ground; therefore, there is a direct path for FH signal transmission from the GS to the aircraft; the multipath effect can be ignored.

For each hop of the FH signal, the GS arranges a dual tone in the baseband, and the frequencies of the dual tone are

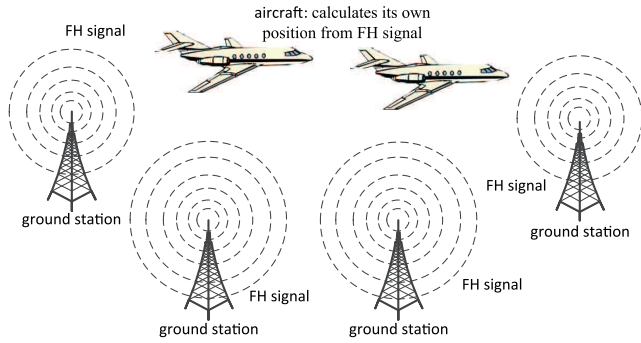


FIGURE 1. A typical APNT system deployment scenario with several GSs and aircrafts.

f_1 and f_2 ($f_1 < f_2$). The dual-tone signals are generated by the same oscillator; therefore, their initial phases are the same. We denote this initial phase by φ_p , where p denotes the GS p . Then, the baseband signal can be expressed as follows:

$$s_p(t) = \sum_{i=1}^2 \exp(j(2\pi f_i(t - \Delta t_k) + \varphi_p)) \quad (1)$$

Multiple aircrafts could be flying in the same area. We assume that all the GSs are mutually time synchronized whereas the time between each GS and the aircraft is not synchronized. Δt_k is the time difference between the GSs and the aircraft k . All GSs are synchronized; therefore, the time difference between the aircraft k and all GSs are the same.

The baseband signal of GS p up-converts to a radio signal by using a carrier with center frequency f_{cp} and the initial phase θ_p :

$$\begin{aligned} s_{p-R}(t) &= a_p s_p(t) \exp(j(2\pi f_{cp}(t - \Delta t_k) + \theta_p)) \\ &= a_p \sum_{i=1}^2 \exp(j(2\pi(f_i + f_{cp})(t - \Delta t_k) + \varphi_p + \theta_p)) \end{aligned} \quad (2)$$

where a_p is the real-valued amplitude of the dual-tone signal. The FH signal changes the carrier center frequency f_{cp} to correspond with the pseudo-random sequence. If the distance between GS p and the aircraft k is d_{pk} , then the propagation delay is d_{pk}/c . The aircraft k receives the signal and down-converts it to the baseband signal by using a carrier with the center frequency f_{ck} and the initial phase η_k :

$$\begin{aligned} r_{pk}(t) &= \beta_{pk} s_{p-R}(t - d_{pk}/c) \exp(j(2\pi(-f_{ck})t + \eta_k)) + w_{pk}(t) \\ &= \beta_{pk} a_p \sum_{i=1}^2 \exp(j(2\pi(f_i + f_{cp} - f_{ck})t + \alpha_i)) + w_{pk}(t) \end{aligned} \quad (3)$$

$$\begin{aligned} \alpha_i &= -2\pi(f_i + f_{cp})(\Delta t_k + d_{pk}/c) \\ &\quad + \varphi_p + \theta_p + \eta_k \pmod{2\pi} \end{aligned} \quad (4)$$

where the complex coefficient β_{pk} denotes the flat-fading channel between the GS p and the aircraft k . The coefficient can be modeled as a zero-mean complex Gaussian random

variable with the variance σ_{pk}^2 . The noise term $w_{pk}(t)$ is modeled as a zero-mean complex Gaussian random process with the variance σ^2 . The signal phase is α_i when the signal is received.

High-performance Direct Digital Synthesizer (DDS), Phase Locked Loop (PLL) [19], and crystal oscillators [20] can be used to synthesize high-precision frequency signals in APNT. The baseband signal can be synthesized by DDS and PLL having a high-precision crystal oscillator, which can produce a baseband signal with accurate frequency. Therefore, the frequency offset of the dual-tone in the baseband can be ignored. On the contrary, there may be a carrier frequency offset (CFO) between f_{cp} and f_{ck} .

B. DOPPLER-EFFECT MODEL

When there is relative movement between the aircraft and the GS, the influence of the Doppler effect needs to be considered. When the relative speed between the GS and the aircraft v satisfies $v \ll c$, the relationship between the Doppler shift f_D and the transmission frequency f_0 is given as follows:

$$f_D = f_0(v/c) \quad (5)$$

When the baseband has a small bandwidth, the Doppler shift difference of the dual-tone is negligible. For example, let us assume that the maximum relative speed of the aircraft and the GS is 440 m/s [21]. If the bandwidth of the baseband is 500 kHz, the Doppler shift difference between the two tones is approximately 0.7 Hz. Therefore, both tones of the dual-tone signal have equal Doppler shifts. The dual-tone interval is constant in the ranging process. The Doppler effect causes the signal received by the aircraft to shift; therefore, the carrier frequency of GS p received by the aircraft can be written as follows:

$$f'_{cp} = f_D + f_{cp} \quad (6)$$

Now, we rewrite (3) and (4) as follows:

$$\begin{aligned} r_{pk}(t) &= \beta_{pk} a_p \sum_{i=1}^2 \exp(j(2\pi(f_i + f'_{cp} - f_{ck})t + \alpha_i)) \\ &\quad + w_{pk}(t) \end{aligned} \quad (7)$$

$$\begin{aligned} \alpha_i &= -2\pi(f_i + f'_{cp})(\Delta t_k + d_{pk}/c) \\ &\quad + \varphi_p + \theta_p + \eta_k \pmod{2\pi} \end{aligned} \quad (8)$$

III. FROM DUAL-TONE RANGE TO TFMR

The fundamental concern of this paper is to determine a ranging method based on high-speed FH signals. Ranging methods have a number of limitations because of the short resident time and the limited instantaneous bandwidths of high-speed FH signals. To resolve this problem, we first introduce dual-tone ranging (DTR) [22], [23]. DTR is an improvement to Radio Interferometric Positioning System (RIPS) [24], [25]. RIPS is used in wireless sensor network (WSN) and it needs four nodes with two senders and two receivers to participate

in ranging process to get the Qrange which is the distance combination between the four nodes. Therefore, the ranging process of RIPS is complicated. Furthermore, there is Qrange ambiguity in RIPS [26], [27] and the UMR of RIPS will limit the coverage of the system. DTR use one sender and one receiver to get the pseudorange between the two nodes and the ranging process is simplified. But the pseudorange ambiguity still exists. DTR and RIPS are mainly applied to WSN, and the coverage of WSN is small relative to the APNT system for aviation. Therefore, smaller UMR can be accepted in WSN but not be accepted in APNT system. DTR can not be directly apply to the APNT system, so, we propose the TFMR method. The proposed TFMR uses different dual tones in different hops, and it constructs a TFM by using multi-hop signals to estimate a pseudorange, which can have a high precision in large areas.

A. DUAL-TONE RANGING

For high-speed FH signals, the initial carrier phases at different hops are different; however, they are the same in the same hop. Therefore, they can be eliminated by a phase difference. The phase difference between the two tones can be expressed as:

$$\Delta\alpha_{pk} = -\alpha_2 + \alpha_1 = 2\pi (f_2 - f_1) (d_{pk}/c + \Delta t_k) \pmod{2\pi} = 2\pi \Delta f d'_{pk}/c \pmod{2\pi} \tag{9}$$

where $\Delta f = f_2 - f_1$, d'_{pk} represents the pseudorange between the GS p and the aircraft k , which is the same as the pseudorange in the GPS.

Then, the pseudorange can be obtained by (10):

$$d'_{pk} = c\Delta\alpha_{pk}/(2\pi\Delta f) + nc/\Delta f \tag{10}$$

where n is an integer and $n \geq 0$, and $c/\Delta f$ is the UMR. When d'_{pk} is larger than UMR, there is ambiguity about d'_{pk} . Therefore, to minimize ambiguity, the UMR should be made as large as possible. Δf determines the UMR. The smaller the Δf , the larger the UMR; however, the accuracy of the range decreases as the Δf decreases [23]. Due to the wide coverage of the APNT system for aviation and the FAA requirements for the APNT system, it requires high-ranging accuracy along with large UMR when the methods similar to DTR are applied to the APNT system. Therefore, the DTR method cannot be directly applied to the APNT system.

B. TIME-FREQUENCY MATRIX RANGING

To improve the UMR, an intuitive approach is to employ a multi-tone within one hop. However, mutual interferences arise among the multiple tones, and these interferences increase as the frequency interval among the multiple tones decrease [28]. The instantaneous bandwidth of the high-speed FH signal is narrow. If the number of tones of the multi-tone signal is increased, the frequency interval among the multiple tones cannot be kept large.

The TFMR proposed by us is shown in Fig. 2. The basic idea in our TFMR is to combine different dual

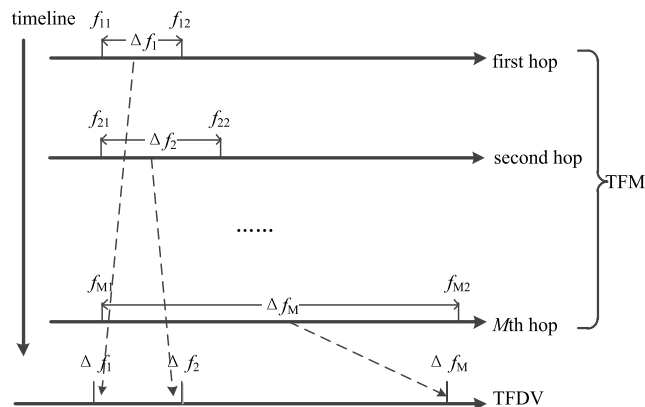


FIGURE 2. The proposed TFM.

tones in different hops and different times to form a TFM. The TFMR transmits dual-tone signals per hop, which minimizes the impact of the narrow instantaneous bandwidth of high-speed FH signals used for ranging. At the same time, the multi-hop signal is combined so that the UMR is improved.

The TFM can be formalized as follows:

$$TFM = \begin{bmatrix} f_{11} & f_{12} \\ f_{21} & f_{22} \\ \dots & \dots \\ f_{M1} & f_{M2} \end{bmatrix}_{M \times 2} \tag{11}$$

where M is the number of rows of the TFM. The frequency of the first tone is the same for all hops, and $f_{i2} > f_{j2}$ if $i > j$. From (8), we can obtain the phase α_{ij} at each measurement frequency. Then these phases can constitute the following time-phase matrix (TPM):

$$TPM = \begin{bmatrix} \alpha_{11} & \alpha_{12} \\ \alpha_{21} & \alpha_{22} \\ \dots & \dots \\ \alpha_{M1} & \alpha_{M2} \end{bmatrix}_{M \times 2} \tag{12}$$

From (9), we can obtain the Time-Frequency Differential Vector (TFDV) and the corresponding Time-Phase Differential Vector (TPDV) as follows:

$$TFDV = [\Delta f_1, \dots, \Delta f_i, \Delta f_{i+1}, \dots, \Delta f_M], \Delta f_i < \Delta f_{i+1} \tag{13}$$

$$TPDV = [\Delta\alpha_1, \dots, \Delta\alpha_i, \Delta\alpha_{i+1}, \dots, \Delta\alpha_M] \tag{14}$$

If we consider each element in TFDV as a measurement frequency, then TFDV contains a series of measurement frequencies, and TPDV can be seen as the phase obtained at this series of measurement frequencies. Therefore, the TFMR can be equivalent to the multi-frequency phase measurement problem [24]. We can obtain a relationship between TFDV and TPDV as shown in (15). By making multiple measurements with different frequencies, we can reconstruct the value of d'_{pk} as follows:

$$\Delta\alpha_i = 2\pi \Delta f_i d'_{pk}/c \pmod{2\pi} \tag{15}$$

Let $\Delta f'_i = \Delta f_{i+1} - \Delta f_i (1 < i < M - 1)$, then $[\Delta f'_1, \dots, \Delta f'_{M-1}]$ can be viewed as the interval of measurement frequency. Reference [18] pointed out that the UMR is inversely proportional to the greatest common divisor (GCD) f_{gcd} of the measurement frequency interval, as shown in (16). Therefore, the TFM can be designed to improve the UMR as follows:

$$UMR = c/f_{gcd} \tag{16}$$

C. MEASUREMENT BANDWIDTH AND SOLUTION BANDWIDTH

We define the TFMR measurement bandwidth B_m as the difference between the highest frequency and the lowest frequency components in the TFM:

$$B_m = \max(f_{ij}) - \min(f_{ij}), 1 \leq i \leq M, 1 \leq j \leq 2 \tag{17}$$

The TFMR method employs Δf_i as the measurement frequency to estimate the pseudorange. Therefore, we define the solution bandwidth B_s of the TFMR as follows:

$$B_s = \max(\Delta f_i) - \min(\Delta f_i), 1 \leq i \leq M \tag{18}$$

The above definition implies that $B_m > B_s$. Let the instantaneous bandwidth of the FH signal be B_i , then $B_i = B_m + f_{11}$. Therefore, B_i limits B_m and B_s .

D. TFM DESIGN

Two aspects need to be taken into account for the TFM design: ranging accuracy and UMR. The tones of a dual-tone signal show mutual interference. To obtain high accuracy, we must select the appropriate frequency interval of the dual-tone signal (Δf). In addition, to make full use of the signal bandwidth, B_s needs to have the highest possible value.

Let T_r denote the resident time of the FH signal. When two tones of the dual-tone signal are orthogonal, their mutual interference is minimum. In other words, Δf is preferably an integer multiple of $1/T_r$. We define $1/T_r$ as the minimum frequency interval (MFI). Then, MFI is the minimum value that can be achieved by the GCD of the frequency interval in TFDV. Thus, MFI limits the UMR (as seen in (16)). With the increase of the hopping speed of the FH signal, T_r decreases so that the UMR also decreases. As Δf increases, the interference between the two tones gradually reduces [28]. We observe the effect of the change of Δf on the phase difference estimation by simulation(see Fig. 3). In the simulation, the sampling time is 100 μ s. The root mean square error (RMSE) of the phase difference estimation is small and similar when Δf exceeds MFI. Therefore, to improve the UMR, we can adopt a compromise scheme, that is, when Δf exceeds MFI, Δf need not necessarily be an integer multiple of MFI.

We provide a TFM generation algorithm to generate a feasible TFM. Given f_{gcd} , B_i , f_{11} , and M , the TFM generation algorithm can be given in the following steps:

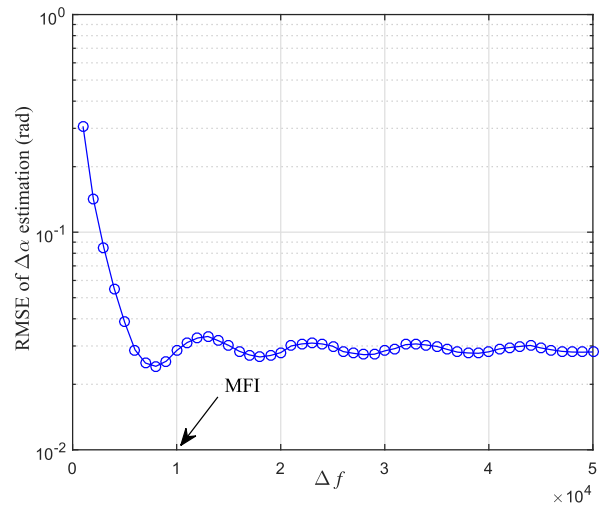


FIGURE 3. The impact of Δf on phase difference estimation.

- 1: Determining f_{12} and f_{M2} , where $f_{12} = f_{11} + n \times MFI$, $f_{M2} = B_i$, which make B_s as large as possible; n is an integer(usually equal to 1).
- 2: Randomly generate two small primes $p1$ and $p2$ such that $f_{22} = f_{12} + f_{gcd} \times p1, f_{32} = f_{22} + f_{gcd} \times p2$.
- 3: Randomly generate the second tone frequency $f_{i2}(i = 4, \dots, M - 1)$ of all other hops within $f_{32} - f_{gcd}$ and $f_{M2} - f_{gcd}$.

E. TFM EXAMPLE

To support the area navigation, APNT needs to have a range of hundreds of kilometers. From (16), if f_{gcd} is 1 kHz, then the UMR is 300 km, which meets the requirement of APNT. Therefore, as an example, we design TFM to make the GCD of TFDV equal to 1 kHz. The hopping speed of the FH signal is 16000 hops/s, and the instantaneous bandwidth $B_i = 100$ kHz. The duration of each hop of the FH signal is called the hop cycle; the duration includes the frequency switching time and the frequency resident time. If we assume that the frequency switching time occupies 20% of the hop cycle, then the frequency resident time $T_r = 0.05$ ms, and the MFI is 20 kHz. In TFM, if $f_{11} = 10$ kHz, $f_{12} = 30$ kHz, $M = 5$, then $f_{52} = 100$ kHz. The frequencies of other hops in the TFM are generated randomly as described above. For example, if TFM = [10, 30; 10, 41; 10, 60; 10, 84; 10, 100] kHz, then TFDV = [20, 31, 50, 74, 90] kHz, and the frequency interval of TFDV is [11, 19, 24, 16]kHz. The GCD of the frequency interval of TFDV f_{gcd} is 1kHz, and the UMR is 300 km. It can also be noted from the above examples that the average frequency interval of the TFDV is less than that of the MFI. However, from the TFM, we can see that the Δf at each hop is larger than that of the MFI, which reduces mutual interference between the different tones. When M increases, this situation will become more obvious.

IV. PSEUDORANGE ESTIMATION

To obtain the pseudorange, the dual-tone phase difference must be estimated; this requires signal frequency information.

The Doppler shift and CFO make it impossible to obtain accurate frequency information. From Section III, we know that the interval of the dual-tone signal remains almost constant during the ranging process. Using this prior knowledge, we propose a frequency-estimation method in this section. After obtaining the dual-tone phase difference, we transform the pseudorange estimation into a single-tone frequency estimation problem. Then, we use the efficient algorithm of the single-tone frequency estimation to estimate the pseudorange.

A. FREQUENCY ESTIMATION BASED ON PRIOR KNOWLEDGE

In the classical multi-tone estimation problem, there is no relationship among the multiple tones; therefore, the frequency of each tone needs to be independently estimated. However, the interval of a dual-tone signal is almost constant in the ranging process. This prior knowledge can be used in estimating the pseudorange.

Inspired by the above observation, we propose a frequency-estimation method based on prior knowledge. For convenience, in (7), let $f_{pki} = f_i + f'_{cp} - f_{ck} (i = 1, 2)$. The frequency of each tone of the baseband signal f_{pki} is obtained by the aircraft; this frequency contains the Doppler shift and the CFO. Firstly, estimating f_{pki} by using the high-resolution frequency-estimation method root-MUSIC [29], we obtain the estimated value \hat{f}_{pki} . The value of f_i is exactly known; therefore, based on f_i and \hat{f}_{pki} we can obtain the frequency offset on each tone. Secondly, by averaging the frequency offset on each tone, we obtain f_O , as shown in (19). The interval of the dual tone is almost constant; therefore, the frequency shift of each tone is the same and is equal to f_O . Finally, based on f_i and f_O , we obtain f'_{pki} , which is employed to estimate the phase difference $\Delta\alpha_{pk}$, as shown in (20).

$$f_O = \sum_{i=1}^2 (\hat{f}_{pki} - f_i) / 2 \tag{19}$$

$$f'_{pki} = f_O + f_i, \quad 1 \leq i \leq 2 \tag{20}$$

B. PHASE DIFFERENCE ESTIMATION OF DUAL-TONE SIGNAL

We estimate the dual-tone phase difference $\Delta\alpha_{pk}$ by using the least squares estimation method. Let us assume that the received signal is converted by AD by using the sampling frequency f_s . Then, we obtain the sample vector r_{pk} containing N samples as follows:

$$r_{pk} = A_{pk} x_{pk} \tag{21}$$

where $A_{pk} = [\Phi(f'_{pk1}/f_s)\Phi(f'_{pk2}/f_s)]$ with $\Phi(f) = [1, \exp(j2\pi f), \dots, \exp(j2\pi(N-1)f)]^T$, and $x_{pk} = \beta_{pk} a_p [\exp(j\alpha_1), \exp(j\alpha_2)]^T$. Then, the least squares estimator of x_{pk} is

$$\hat{x}_{pk} = (A_{pk})^\dagger r_{pk} \tag{22}$$

The estimator of $\Delta\alpha_{pk}$ is

$$\Delta\hat{\alpha}_{pk} = \arg \{ [\hat{x}_{pk}]_1 [\hat{x}_{pk}]_2^* \} \tag{23}$$

where the operators $[\cdot]^T$, $[\cdot]^*$, and $(\cdot)^\dagger$ denote the transpose, the complex conjugate, and the generalized inverse. The i th element of vector a is denoted by $[a]_i$.

C. USING TFM TO ESTIMATE PSEUDORANGE

Reference [30] and [31] shows that the additive white Gaussian complex noise of single-tone signal can be converted into an equivalent additive white Gaussian noise of phase in large signal-to-noise ratio (SNR). Therefore, the noise of α_i in (7) can be modeled as a zero-mean Gaussian noise. As show in Section III, the RMSE of the phase difference estimation is small and similar when Δf exceeds MFI. In the TFM generated by the TFM generation algorithm, Δf_i is larger than MFI. Therefore, it can be assumed that the tones of dual-tone signals in TFM are independent of each other. So, in large SNR, (15) can be modeled as:

$$\Delta\alpha_i = 2\pi \Delta f_i d'_{pk} / c + n_i \pmod{2\pi} \tag{24}$$

where n_i is modeled as a zero-mean Gaussian noise with the variance σ_α^2 .

Then, we present the maximum likelihood (ML) estimator of pseudorange of the TFMR method. In large SNR, (24) can be converted into an equivalent form [30], [31]:

$$\exp(j\Delta\alpha_i) = \exp(j2\pi d'_{pk} \Delta f_i / c) + z_i \tag{25}$$

where z_i is complex white Gaussian noise with variance $2\sigma_\alpha^2$. Then the pseudorange estimation of the TFMR method is equivalent to a single-tone frequency estimation and we can regard d'_{pk} as the frequency of a single tone and $\Delta f_i / c$ as the discrete sample time.

However, the interval between the Δf_i may be uniform or non-uniform. When the interval between Δf_i is uniform, the pseudorange estimation of the TFMR method is equivalent to the single-tone estimation with uniform sampling. Then, the ML estimator for the pseudorange d'_{pk} is

$$\hat{d}'_{pk} = \arg \max_d \left\{ \prod_{i=0}^{M-1} \exp(j\Delta\hat{\alpha}_i) \exp(-j2\pi \Delta f_i d / c) \right\} \tag{26}$$

where $\Delta\hat{\alpha}_i$ is the estimated value of the phase difference in TPDV. When the interval between Δf_i is non-uniform, it is equivalent to the single-tone estimation with non-uniform sampling [32]. Let the minimum frequency resolution be f_{min} , and the minimum value of Δf_i be $n \times f_{min}$. B_s is L times f_{min} , where k, n and L are integers. Then, the maximum likelihood estimator for the pseudorange d'_{pk} is

$$\hat{d}'_{pk} = \arg \max_d \left\{ \prod_{k=0}^{L-1} \exp(j\Delta\hat{\alpha}_k) \exp(-j2\pi (k+n)f_{min} d / c) \right\} \tag{27}$$

In (27), if we insert a number of measurement frequencies to transform the single-tone estimation with non-uniform sampling problem into a uniform sampling problem, then, $L > M$. The estimated value of the phase difference for

the inserted measurement frequency should be made zero. We have solved (26) and (27) by using the FFT-based dichotomous search method proposed in [33] because it provides an efficient solution.

V. CRAMER-RAO LOWER BOUND

In this section, we derive the CRLB for TFMR based on the models described in (7) and (25). In order to estimate the pseudorange, we first obtain the phase difference by the least squares estimator in (23), then we use the estimation of the phase difference to estimate the pseudorange by ML estimator in (26) and (27). Although we use the least squares estimator to estimate phase difference, the least squares estimator is equivalent to ML estimator when the noise is Gaussian [30]. So, we first derive CRLB for the phase difference and then derive CRLB for the pseudorange.

A. CRLB FOR THE PHASE DIFFERENCE

The tones of dual-tone signals in TFM can be regarded as independent of each other. Therefore, we convert the dual-tone signal parameter estimation problem into two single-tone parameter estimation problems. According to (7), the independent single-tone signal can be modeled as:

$$r_{pki}(t) = \beta_{pk} a_p \exp(j(2\pi f_{pki}t + \alpha_i)) + w_{pk}(t) \quad (28)$$

For the first tone of dual-tone signal, $r_{pk1}(t)$ ($i = 1$) is converted by AD with sampling frequency f_s and the sample vector is $R = [r_{pk1,0}, r_{pk1,1}, \dots, r_{pk1,N-1}]$ with N samples. Then, the joint probability density function (pdf) of the elements of the sample vector R when the unknown parameter vector is $\Gamma = [\omega_1, a_p, \alpha_1, \beta_{re}, \beta_{im}]^T$ is given by

$$f(R; \Gamma) = \left(\frac{1}{\sigma^2 \pi}\right)^N \times \exp\left[-\frac{1}{\sigma^2} \sum_{n=0}^{N-1} (X_n - \mu_n)^2 + (Y_n - v_n)^2\right] \quad (29)$$

where $X_n = Re(r_{pk1,n})$, $Y_n = Im(r_{pk1,n})$, $\beta_{re} = Re(\beta_{pk})$, $\beta_{im} = Im(\beta_{pk})$, $\omega_1 = 2\pi f_{pk1}$, σ^2 is the variance of the complex Gaussian random process $w_{pk}(t)$. u_n and v_n is:

$$u_n = a_p (\beta_{re} \cos(\omega_1 nT + \alpha_1) - \beta_{im} \sin(\omega_1 nT + \alpha_1)) \quad (30)$$

$$v_n = a_p (\beta_{re} \sin(\omega_1 nT + \alpha_1) + \beta_{im} \cos(\omega_1 nT + \alpha_1)) \quad (31)$$

where T is $1/f_s$.

Since the unknown parameter β_{pk} is a zero-mean complex Gaussian random variable with the variance σ_{pk}^2 , then β_{re} and β_{im} are zero-mean Gaussian random variable with the variance $\sigma_{pk}^2/2$. Therefore, the parameter vector Γ consists of both random and non-random parameters and hybrid CRLB (HCRLB) can be derived [34]:

$$HCRLB = \begin{bmatrix} CRLB_{\Gamma_1} & 0 \\ 0 & BCRLB_{\Gamma_2} \end{bmatrix} \quad (32)$$

where $\Gamma_1 = [\omega_1, a_p, \alpha_1]^T$ and $\Gamma_2 = [\beta_{re}, \beta_{im}]^T$ represent non-random and random parameters of Γ respectively.

$BCRLB_{\Gamma_2}$ is Bayesian CRLB of random parameters in Γ_2 . We only care about $CRLB_{\Gamma_1}$ and the Fisher Information Matrix (FIM) is

$$\begin{aligned} J_D &= E_{\Gamma_2} [J_{\Gamma_1}] \\ &= E_{\Gamma_2} \left[\frac{2(\beta_{re}^2 + \beta_{im}^2)}{\sigma^2} \begin{bmatrix} a_p^2 T^2 Q & 0 & a_p^2 TP \\ 0 & N & 0 \\ a_p^2 TP & 0 & a_p^2 N \end{bmatrix} \right] \\ &= \frac{2\sqrt{2}\sigma_{pk}}{\sigma^2} \begin{bmatrix} a_p^2 T^2 Q & 0 & a_p^2 TP \\ 0 & N & 0 \\ a_p^2 TP & 0 & a_p^2 N \end{bmatrix} \end{aligned} \quad (33)$$

where J_{Γ_1} denotes FIM with unknown parameters Γ_1 , E_{Γ_2} is the expectation with respect to Γ_2 , P and Q are as follow:

$$P = \sum_{n=0}^{N-1} n = \frac{N(N-1)}{2} \quad (34)$$

$$Q = \sum_{n=0}^{N-1} n^2 = \frac{N(N-1)(2N-1)}{6} \quad (35)$$

Then the CRLB of α_1 is

$$CRLB_{\alpha_1} = [J_D^{-1}]_{33} = \frac{\sqrt{2}\sigma^2(2N-1)}{4\sigma_{pk}a_p^2N(N+1)} \quad (36)$$

The CRLB of α_2 is the same as the CRLB of α_1 . Then the CRLB of $\Delta\alpha_{pk}$ with unknown ω_1, ω_2 ($\omega_2 = 2\pi f_{pk2}$) and a_p is

$$CRLB_{\Delta\alpha_{pk}} = CRLB_{\alpha_1} + CRLB_{\alpha_2} = \frac{\sqrt{2}\sigma^2(2N-1)}{2\sigma_{pk}a_p^2N(N+1)} \quad (37)$$

Although the frequencies of the dual-tone signal are unknown, the frequency difference between the two tones of dual-tone signal in each row of TFM is known. This prior knowledge is used to estimate the frequencies of dual-tone signal in (19) and (20). Part of the frequency information is used to estimate the phase difference. Therefore, when we derive CRLB for the phase difference, it is not appropriate to regard ω_1 and ω_2 as unknown parameters. Then, when we estimate α_1 , the unknown parameter vector is $\Gamma' = [a_p, \alpha_1, \beta_{re}, \beta_{im}]^T$ and the joint pdf of the elements of the sample vector R is the same in (29). The FIM of non-random parameters in Γ' is

$$\begin{aligned} J'_D &= E_{\Gamma'_2} [J_{\Gamma'_1}] \\ &= E_{\Gamma_2} \left[\frac{2(\beta_{re}^2 + \beta_{im}^2)}{\sigma^2} \begin{bmatrix} N & 0 \\ 0 & a_p^2 N \end{bmatrix} \right] \\ &= \frac{2\sqrt{2}\sigma_{pk}}{\sigma^2} \begin{bmatrix} N & 0 \\ 0 & a_p^2 N \end{bmatrix} \end{aligned} \quad (38)$$

Then the CRLB of α_1 with known ω_1 is

$$CRLB'_{\alpha_1} = [J_{\Gamma'_1}^{-1}]_{22} = \frac{\sqrt{2}\sigma^2}{4\sigma_{pk}a_p^2N} \quad (39)$$

The CRLB of $\Delta\alpha_{pk}$ with known ω_1, ω_2 and unknown a_p is

$$CRLB'_{\Delta\alpha_{pk}} = \frac{\sqrt{2}\sigma^2}{2\sigma_{pk}a_p^2N} \quad (40)$$

B. CRLB FOR THE PSEUDORANGE

In (20), when ω_1 and ω_2 are unknown, $\sigma_\alpha^2 \geq CRLB_{\Delta\alpha}$ and when ω_1 and ω_2 are known, $\sigma_\alpha^2 \geq CRLB'_{\Delta\alpha}$. Therefore, in order to derive CRLB for the pseudorange, we can regard $CRLB_{\Delta\alpha}$ and $CRLB'_{\Delta\alpha}$ as σ_α^2 in different situations.

Let the observation of TPDV is $\Delta\Phi = [\Delta\alpha_1, \dots, \Delta\alpha_M]$, $\Delta F = [\Delta f_1, \dots, \Delta f_M]$ and $\Omega = \exp(j\Delta\Phi)$, then the joint pdf of Ω at ΔF with the unknown parameter vector $B = [d'_{pk}]$ is

$$f(\Omega; B) = \left(\frac{1}{2\pi\sigma_\alpha^2}\right)^M \times \exp\left[-\frac{1}{2\sigma_\alpha^2} \sum_{i=1}^M (a_i - u_i)^2 + (b_i - v_i)^2\right] \quad (41)$$

where $a_i = \text{Re}(j\Delta\alpha_i)$, $b_i = \text{Im}(j\Delta\alpha_i)$, $u_i = \cos\left(2\pi\frac{\Delta f_i}{c}d'_{pk}\right)$, $v_i = \sin\left(2\pi\frac{\Delta f_i}{c}d'_{pk}\right)$.

The CRLB of d'_{pk} is

$$CRLB = -1 \left/ E \left[\frac{\partial^2 f(\Omega; B)}{\partial d'_{pk}{}^2} \right] \right. = \sigma_\alpha^2 c^2 \left/ \sum_{i=1}^M 4\pi^2 \Delta f_i^2 \right. \quad (42)$$

Then, according to (37) and (40), the CRLB of d'_{pk} without and with frequency knowledge of dual-tone signal are

$$CRLB_d \geq \frac{\sqrt{2}c^2\sigma^2(2N-1)}{8\pi^2\sigma_{pk}a_p^2N(N+1)} \left/ \sum_{i=1}^M \Delta f_i^2 \right. \quad (43)$$

$$CRLB'_d \geq \frac{\sqrt{2}c^2\sigma^2}{8\pi^2\sigma_{pk}a_p^2N} \left/ \sum_{i=1}^M \Delta f_i^2 \right. \quad (44)$$

VI. SIMULATION RESULTS

In the simulation, let us first consider the ideal situation where there is no CFO and Doppler shift, that is, the frequency of received signal is exactly known. Subsequently, the CFO and the Doppler shift are considered, which means the frequency of the received signal is unknown and must be estimated. And, we analyzed the impact of the bandwidth, TFM rows, and the sampling frequency on the ranging performance. Furthermore, the robustness of TFMR is analyzed. To analyze the ranging performance of the TFMR, we did not take into account the time difference between the GS and the aircraft, that is, $\Delta t_k = 0$. Therefore, we do not distinguish between the pseudorange and the distance in the simulation. The central frequency of the FH signal carrier is in the range of 1 GHz to 1.5 GHz in the simulation, and the amplitude of the dual-tone signal $a_p = 1$. Moreover, the average channel power of the flat-fading channel is always assumed to be 1, therefore $\sigma_{pk}^2 = 1$.

TABLE 1. Parameters of the FH signal.

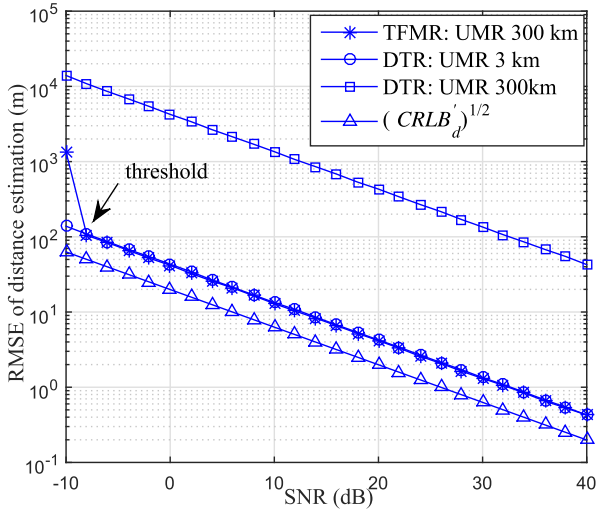
Parameter name	Parameter 1	Parameter 2
Hopping speed	800 hop/s	16000 hop/s
Hop cycle	1.25ms	0.0625ms
Resident time T_r	1ms	0.05ms
Instantaneous bandwidth B_i	110kHz	110kHz
Sampling frequency f_s	250kHz	250kHz
The number of rows of TFM	10	10
Frequency of first tone f_{i1}	10 kHz	10 kHz

A. SIGNAL WITHOUT CFO AND DOPPLER SHIFT TO EVALUATE RANGING PERFORMANCE

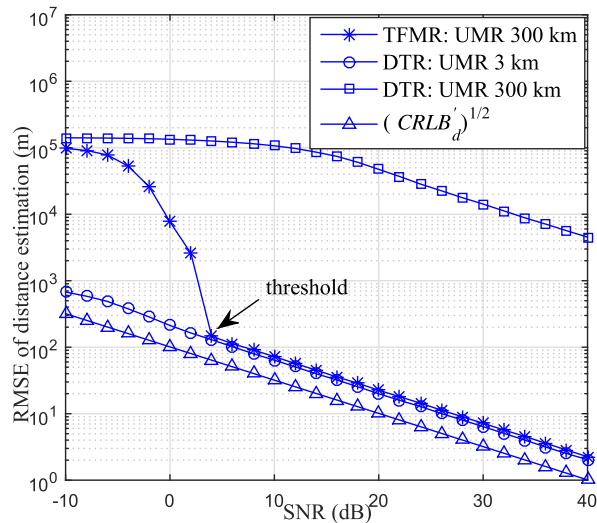
When there is no CFO and Doppler shift with received signal, the frequency of the received signal is accurately known. We compare the ranging accuracy and UMR between the DTR and the TFMR. When the DTR is used for FH signals, the same dual tone is transmitted at each hop, and the estimated distance of M hops are averaged. In the DTR, the frequency of the first tone f_1 is 10 kHz, and the frequency differences between the two tones are 100 kHz and 1 kHz, which correspond to the UMRs of 3 km and 300 km, respectively. The distance between the GS and the aircraft is 1.3 km.

The default parameters of the FH signal are shown in Table 1. We simulated low-speed and high-speed FH signals in which the frequency switching time was taken as 20% of the hop cycle. The distance between the GS and aircraft is 200 km. Reference [35] pointed out that the instantaneous bandwidth of the FH signal is between several kHz and several MHz; therefore, we set the instantaneous bandwidth to 110 kHz. We analyzed the average performance of the TFMR under different TFMs, which were randomly generated based on Section III. When the hopping speed was 800 hops/s, $f_{12} = 15$ kHz; when the hopping speed was 16000 hops/s, $f_{12} = 30$ kHz.

The number of Monte Carlo trials is 10^4 for each SNR. As shown in Fig. 4(a), when the hopping speed of the FH signal is 800 hops/s and the UMR of the TFMR and DTR is 300 km, the RMSE of the distance estimation of the TFMR is much less than that of the DTR. For example, when the SNR is 20 dB, the RMSE of distance estimation of the TFMR is approximately 4.16 m, whereas that of the DTR reached 430.9 m. When the interval of the dual-tone is 100 kHz, and the UMR is 3 km in the DTR, the range performances of the TFMR and DTR are almost the same. When the hopping speed is 16,000 hops/s, the situation is similar to what can be seen in Fig. 4(b). However, Fig. 4 shows that the RMSE of the TFMR distance estimation has a threshold effect, and the subsequent simulations show that adjusting the TFMR parameters can reduce the threshold levels. In addition, the square root of the CRLB of the pseudorange estimation is used as benchmark in Fig. 4. Although the RMSE of the TFMR distance estimation is close to $(CRLB'_d)^{1/2}$, there is performance gap between them. As pointed out by [23], the deep fading channel can fail the range estimation and causes large errors.



(a)



(b)

FIGURE 4. RMSE of distance estimation when the received signal without CFO and Doppler shift: (a) parameter 1, (b) parameter 2.

B. SIGNAL WITH CFO AND DOPPLER SHIFT TO EVALUATE RANGING PERFORMANCE

The range measurement becomes limited as the hopping speed of the FH signal increases. Therefore, when there is CFO and Doppler shift with received signal, we analyzed the FH signal with the hopping speed of 16000 hops/s. We considered the Doppler shift and the CFO, which adversely impact the ranging. When the maximum relative speed of the aircraft and the GS were approximately 440 m/s, the maximum Doppler shift was approximately 2200 Hz according to the central frequency of the carrier. We can use high-performance devices here, such as OCXO crystals because they have a frequency accuracy of up to 1×10^{-8} [20]. As a result, when the carrier frequency was 1.5 GHz, the maximum

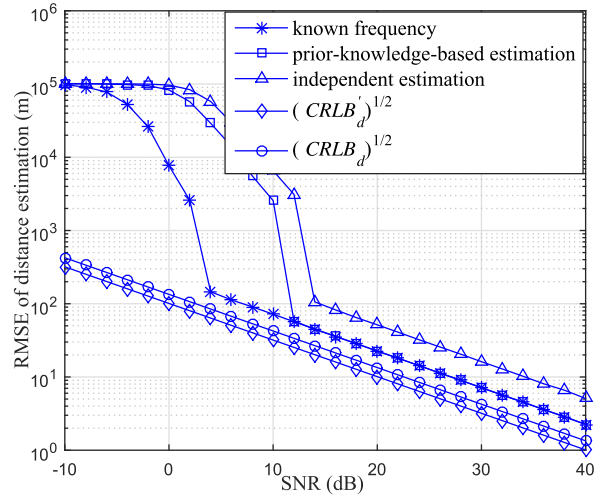


FIGURE 5. RMSE of distance estimation with different frequency-estimation methods.

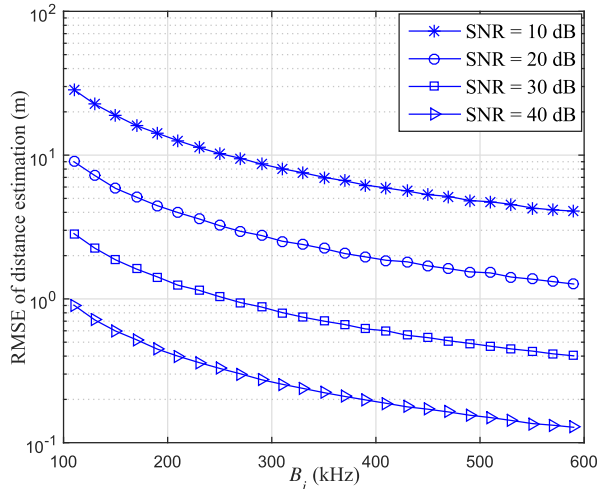
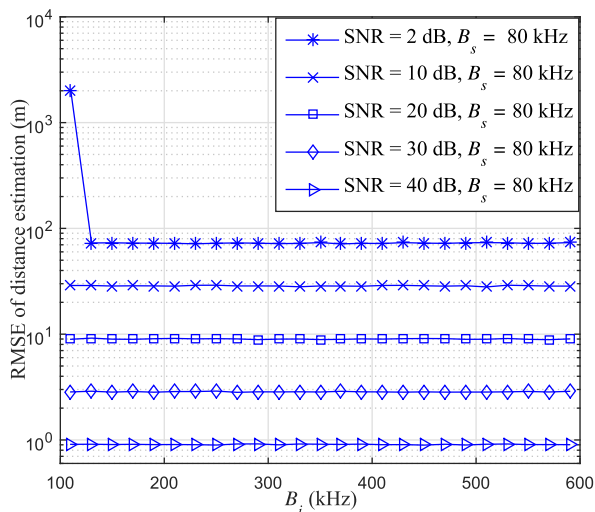


FIGURE 6. RMSE of distance estimation with B_i increasing and f_{12} unchanging ($B_m=B_i-f_{11}$, $B_s=B_i-f_{12}$; therefore, B_m and B_i are increasing).

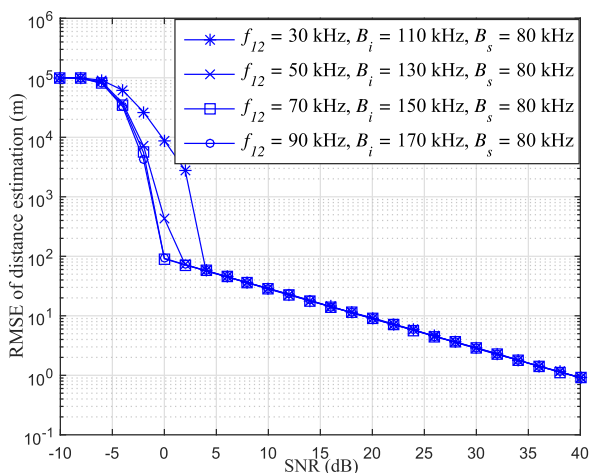
CFO between the GS and the aircraft was approximately 30 Hz. Therefore, in the simulation, we allowed the frequency offset caused by the Doppler shift and the CFO to be uniformly distributed in the range of $[-3, 3]$ kHz. TFM was randomly generated based on Section III. By default f_{12} is 30 kHz.

1) PERFORMANCE ANALYSIS OF PRIOR-KNOWLEDGE-BASED FREQUENCY ESTIMATION

As shown in Fig. 5, when the TFMR adopts the prior-knowledge-based frequency-estimation method, the threshold level of the threshold effect increases more than that of the case in which the frequency is known. However, the RMSE of distance estimation is almost the same from the middle to the high SNR. When the frequency of the dual-tone is independently estimated, the threshold is increased further and also the RMSE of distance estimation from the



(a)



(b)

FIGURE 7. RMSE of distance estimation with B_s kept invariant and B_i and B_m increased: (a) RMSE vs. B_i , (b) RMSE vs. SNR.

middle to the high SNR is greatly increased. For example, when SNR is 20 dB, the RMSE of the distance estimation is approximately 2.3 times as much as the RMSE of the former. In addition, when the frequency of the dual-tone is independently estimated, no frequency information has been used, then the CRLB of distance estimation is $(CRLB_d)^{1/2}$. While the prior-knowledge-based frequency-estimation method is used, some prior knowledge about the frequency of the dual-tone signal are used, then the CRLB of distance estimation is $(CRLB'_d)^{1/2}$. The performance gap between the $(CRLB_d)^{1/2}$ and the RMSE of distance estimation with independently frequency estimation is larger than the performance gap between the $(CRLB'_d)^{1/2}$ and the RMSE of distance estimation with the prior-knowledge-based frequency-estimation. This is because the CFO and Doppler shift can not be correctly estimated when the frequency is independently estimated.

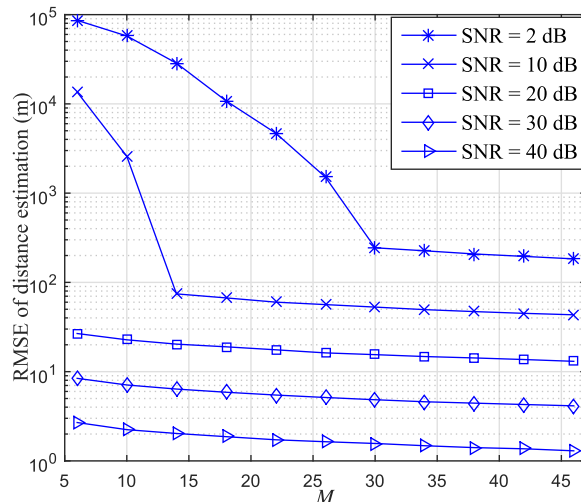


FIGURE 8. RMSE of distance estimation with different number of TFM rows.

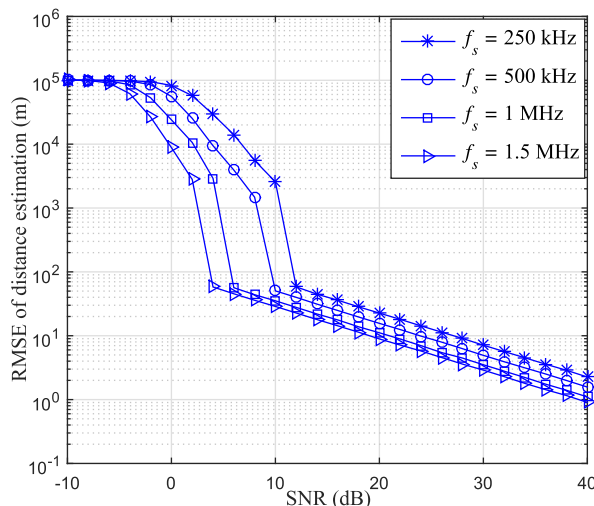
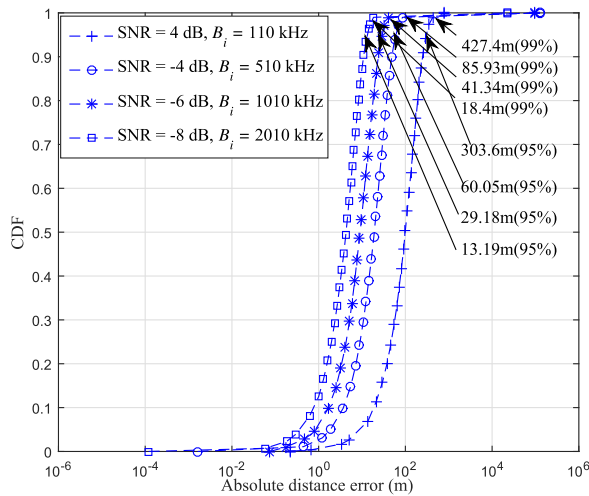


FIGURE 9. RMSE of distance estimation with different sampling frequencies.

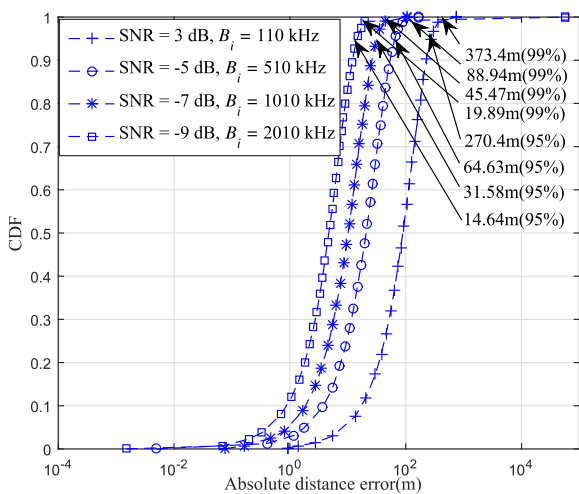
2) IMPACT OF BANDWIDTH, TFM ROWS, AND SAMPLING FREQUENCY ON RANGING PERFORMANCE

We analyzed the impact of the bandwidth on ranging performance. In the simulation, when we increased the instantaneous bandwidth B_i keeping f_{12} unchanged, the measurement bandwidth B_m and the solution bandwidth B_s constantly increased, and B_s was equal to $B_i - f_{12}$. The sampling frequency f_s was 1.5 MHz. As shown in Fig. 6, as the bandwidth increases, the RMSE of distance estimation decreases. It can be seen that increasing the B_i of the FH signal can improve the TFMR ranging performance. However, because B_m and B_s increase simultaneously, we cannot distinguish the impact of them on ranging performance.

To analyze the impact of B_m and B_s on ranging performance, we increased B_i as well as B_m ($B_m = B_i - f_{11}$), but B_s was kept constant, that is, we increased f_{12} and made $B_s = 80$ kHz when B_i was increased. Fig. 7(a), shows that increasing B_m has little effect on the RMSE of distance estimation when B_s is kept invariant. Fig. 6 and Fig. 7(a) show



(a)



(b)

FIGURE 10. CDF curves of the absolute distance error of distance estimation: (a) $M = 30$, (b) $M = 50$.

that B_s is an important parameter for the TFMR. However, B_i limits B_s . To improve the ranging performance, we require both B_i and B_s as large as possible. When SNR is 2 dB, the threshold level of the threshold effect is reduced when B_i and f_{12} are reduced. Fig. 7(b) further confirms this fact. However, there is no effect on the threshold when f_{12} is increased to a certain extent. Fig. 7(b) shows that when $f_{12} = 70$ kHz and $f_{12} = 90$ kHz, the threshold levels of the threshold effects for both are equivalent. Although increasing f_{12} can reduce the threshold level of the threshold effect, it also makes B_s smaller for the same B_i .

We further analyzed the influence of M (the number of rows of TFM) on the distance estimation under the same solution bandwidth. Fig. 8 shows that the RMSE of distance estimation decreases gradually as M increases. In particular, when the SNR values are 2 dB and 10 dB, the threshold level of the threshold effect gradually reduces as M increases. In other words, by increasing the number of TFM

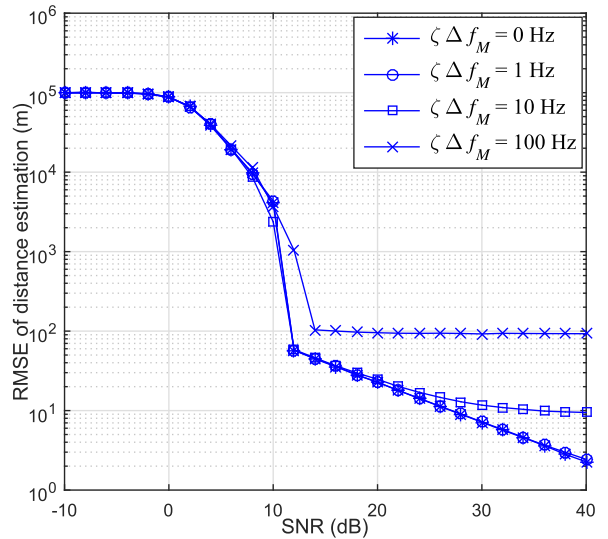


FIGURE 11. RMSE of distance estimation with different frequency discrepancies.

rows, the threshold level of the threshold effect can be reduced.

The signal sampling frequency f_s is also an important parameter affecting the TFMR performance. From Fig. 9, we can see that increasing f_s can reduce both the RMSE of distance estimation and the threshold level of the threshold effect.

3) ANALYSIS OF ABSOLUTE RANGING ERROR

The cumulative distribution function (CDF) curves of the absolute distance error with different TFMR parameters are illustrated in Fig. 10. We used different sampling frequencies for different instantaneous bandwidths. The corresponding values were as follows: $B_i = 110$ kHz, $f_s = 250$ kHz; $B_i = 510$ kHz, $f_s = 1.5$ MHz; $B_i = 1010$ kHz, $f_s = 2.5$ MHz; and $B_i = 2010$ kHz, $f_s = 4.5$ MHz. Fig. 10(a) shows the case in which $M = 30$. When the B_i is 110 kHz, SNR is 4 dB, and the ranging accuracy is the worst—it is less than 303.6 m 95% of the time and less than 427.4 m 99% of the time. This meets the FAA’s requirements for APNT. When B_i is 2010 kHz, SNR is -8 dB, and the accuracy of ranging is best: 13.19 m (95%) and 18.4m (99%). Fig. 10(b) shows the case in which $M = 50$. It can be seen that when M increases, the same ranging accuracy can be obtained with a lower SNR. In short, for ranging accuracy, the TFMR meets the requirements of the APNT system.

4) ROBUSTNESS ANALYSIS OF TFMR

When high-performance DDS, PLL, and crystal oscillators are used, baseband signal with accurate frequency can be produced. The CFO and Doppler shift have almost no effect on the dual-tone interval. However, there are frequency discrepancies on the frequency interval of the dual-tone signal when the devices performance are reduced. So, we add random frequency discrepancies on Δf_i . The frequency discrepancies are uniformly distributed in the range of $[-\zeta \Delta f_i, \zeta \Delta f_i]$, where $\zeta \in \{1000ppm, 100ppm, 10ppm\}$

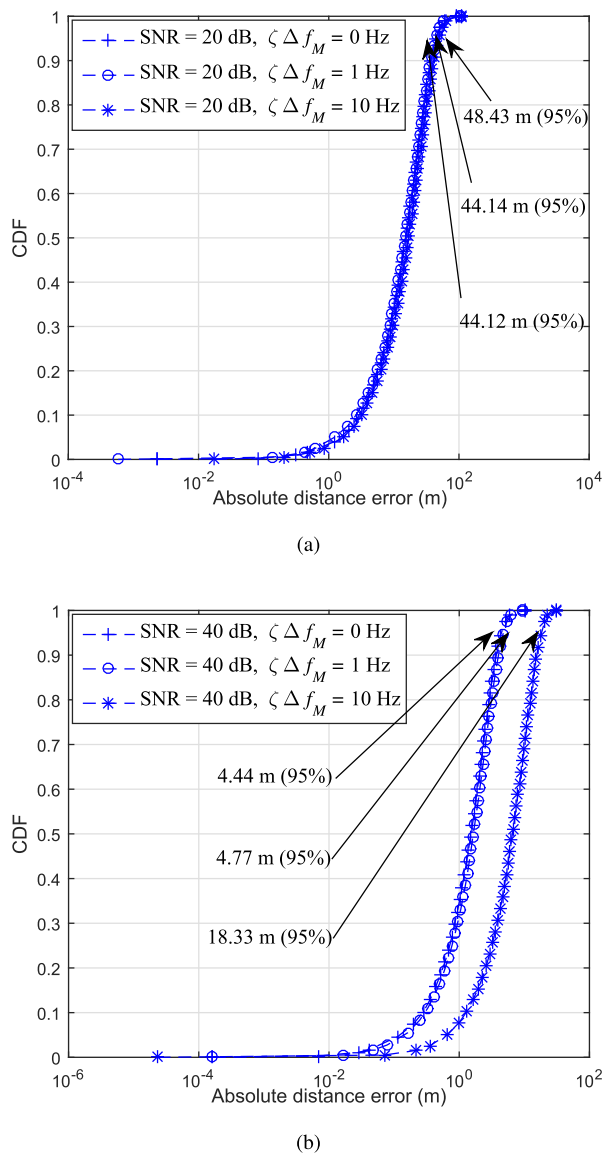


FIGURE 12. CDF curves of the absolute distance error of distance estimation with different frequency discrepancies: (a) SNR = 20 dB, (b) SNR = 40 dB.

($1ppm = 10^{-6}$). In the ranging process of TFMR, the maximum frequency discrepancies will appear in the M th row of TFM. That is, $\zeta \Delta f_M$ is maximum in all $\zeta \Delta f_i$. Therefore, we use $\zeta \Delta f_M$ to show the frequency discrepancies in simulation. Other simulation parameters are the same as in Fig. 5. As $\Delta f_M = 100$ kHz, $\zeta \Delta f_M \in \{1 \text{ Hz}, 10 \text{ Hz}, 100 \text{ Hz}\}$. And $\zeta \Delta f_M = 0$ Hz denotes there is no frequency discrepancy. In short, TFMR is still robust when the maximum frequency discrepancy reaches 10 Hz.

In Fig. 11, when $\zeta \Delta f_M = 1$ Hz, the RMSE of distance estimation is almost equal with the case $\zeta \Delta f_M = 0$ Hz. Frequency discrepancy with 1 Hz has almost no effect on TFMR. This is further confirmed by Fig. 12 which is illustrate the CDF curves of the absolute distance error with different discrepancies in different SNR. The ranging accuary is less than 44.12 m 95% of the time with $\zeta \Delta f_M = 0$ Hz

and 44.14 m 95% of the time with $\zeta \Delta f_M = 1$ Hz in SNR = 20 dB. And the situation is the same as SNR = 40 dB. When $\zeta \Delta f_M = 10$ Hz, with the increase of SNR, the influence of frequency discrepancy on the RMSE of distance estimation becomes more and more significant. The ranging accuary is 48.43 m (95%) with $\zeta \Delta f_M = 10$ Hz and 44.12 m (95%) with $\zeta \Delta f_M = 0$ Hz in SNR = 20 dB. There is a certain gap between the two case, but the gap is not significant. When SNR = 40 dB, the ranging accuary becomes 18.33 m (95%) with $\zeta \Delta f_M = 10$ Hz and 4.44 m (95%) with $\zeta \Delta f_M = 0$ Hz. The gap between the two case is significant, but the ranging accuary also is acceptable when $\zeta \Delta f_M = 10$ Hz. When $\zeta \Delta f_M = 100$ Hz, the RMSE of distance estimation is unacceptable as show in Fig. 11.

VII. CONCLUSION

In this paper, we propose a wireless ranging method for aviation navigation called the TFMR. It has anti-jamming capability and uses high-speed FH signals. In the aviation navigation scene, the GS transmits the FH signal. The aircraft receives the signal and calculates the pseudorange between the GS and the aircraft; this ranging process is passive and makes the system capacity unlimited. Simulation results gave the following results:

- 1) The TFMR can obtain a ranging performance similar to the DTR, but it effectively improves the UMR of the ranging.
- 2) When the Doppler effect and the CFO are present, the frequency-estimation method based on prior knowledge can effectively improve the ranging performance, which makes the TFMR robust.
- 3) The solution bandwidth B_s is an important parameter that affects the TFMR ranging performance, and increasing B_s can reduce the RMSE of distance estimation of the TFMR.
- 4) Increasing the number of TFM rows and the signal sampling frequencies can reduce the RMSE of distance estimation and reduce the threshold level of the threshold effect.
- 5) Increasing f_{12} , that is, increasing the interval of the dual-tone signal of the TFM can reduce the threshold of the threshold effect. However, this method reduces B_s , which results in a decrease in the ranging performance from the middle to the high SNR.
- 6) TFMR is still robust when the maximum frequency discrepancy reaches 10 Hz.

In short, the TFMR uses high-speed FH signals with high anti-jamming ability to realize high-precision ranging and to improve the UMR of ranging. The proposed TFMR meets FAA’s requirements for APNT technologies; therefore, the TFMR can be used as an alternative solution for aviation navigation systems.

REFERENCES

[1] J. Coffed, “The threat of GPS jamming: The risk to an information utility,” EXELIS, Tysons Corner, VA, USA, Tech. Rep., Jan. 2014. [Online]. Available: https://www.harris.com/sites/default/files/downloads/solutions/d0783-0063_threatofgpsjamming_v2_mv.pdf

- [2] Government Accountability Office (GAO), "Alternative positioning, navigation and timing (PNT) study," presented at the Int. Civil Aviation Org. Navigat. Syst. Panel, Working Group Meetings, Montreal, ON, Canada, May 2010.
- [3] D. Shutin, N. Schneckenburger, M. Walter, and M. Schnell, "LDACS1 ranging performance—An analysis of flight measurement results," in *Proc. IEEE/AIAA 32nd Digit. Avionics Syst. Conf. (DASC)*, East Syracuse, NY, USA, Oct. 2013, pp. 3C6-1–3C6-10.
- [4] S. Lo, B. Peterson, D. Akos, M. Narins, R. Loh, and P. Enge, "Alternative position navigation & timing (APNT) based on existing DME and UAT ground signals," in *Proc. Inst. Navigat. GNSS Conf.*, Portland, OR, USA, 2011, pp. 1–9.
- [5] E. Kim, "Investigation of APNT optimized DME/DME network using current state-of-the-art DMEs: Ground station network, accuracy, and capacity," in *Proc. IEEE/ION Position Location Navigat. Symp.*, Myrtle Beach, SC, USA, Apr. 2012, pp. 146–157.
- [6] O.-J. Kim, C. Kim, J. Song, Y. Kim, and C. Kee, "The study of error sources for MOSAIC/DME system: A single station based positioning system for APNT," in *Proc. IEEE/ION Position, Location Navigat. Symp.*, Monterey, CA, USA, May 2014, pp. 855–863.
- [7] T. Ertan and M. L. Psiaki, "Alternative position and navigation based on DME accumulated delta range," *Navigation*, vol. 63, no. 2, pp. 145–159, 2016.
- [8] S. Han, Z. Gong, W. Meng, C. Li, and X. Gu, "Future alternative positioning, navigation, and timing techniques: A survey," *IEEE Wireless Commun.*, vol. 23, no. 6, pp. 154–160, Dec. 2016.
- [9] E. Kim, "Improving DME performance for APNT using alternative pulse and multipath mitigation," *IEEE Trans. Aerosp. Electron. Syst.*, vol. 53, no. 2, pp. 877–887, Apr. 2017.
- [10] O. Osechas and G. Berz, "Improving the availability of LDACS-based APNT with air-to-air ranging," in *Proc. IEEE/ION Position, Location Navigat. Symp.*, Savannah, GA, USA, May 2016, pp. 91–99.
- [11] E. Kim, "Benefit analysis of a GA-based DME/N pulse on PBN," in *Proc. Integr. Commun., Navigat. Surveill. Conf.*, Herndon, VA, USA, Apr. 2017, pp. 1B–4B.
- [12] N. Neji, R. de Lacerda, A. Azoulay, T. Letertre, and O. Outtier, "Coexistence between the future aeronautical system for continental communication L-DACS and the distance measuring equipment DME," in *Proc. IEEE 1st AESS Eur. Conf. Satellite Telecommun. (ESTEL)*, Rome, Italy, Oct. 2012, pp. 1–7.
- [13] W. Hu *et al.*, "COGNITIVE RADIOS FOR DYNAMIC SPECTRUM ACCESS—Dynamic frequency hopping communities for efficient IEEE 802.22 operation," *IEEE Commun. Mag.*, vol. 45, no. 5, pp. 80–87, May 2007.
- [14] R. Zhi, L. Zhang, and Z. Zhou, "Cognitive frequency hopping," in *Proc. Cognit. Radio Oriented Wireless Netw. Commun.*, Singapore, May 2008, pp. 1–4.
- [15] L. Zhidong and Z. Xiaolin, "A novel frequency hopping scheme based on cognitive radio for aircraft," in *Proc. IEEE Int. Conf. IEEE Cyber, Phys. Social Comput. Green Comput. Commun. (GreenCom), IEEE Internet Things (iThings/CPSCom)*, Beijing, China, Aug. 2013, pp. 1231–1236.
- [16] L. Guan, Z. Li, J. Si, and R. Gao, "Generation and characteristics analysis of cognitive-based high-performance wide-gap FH sequences," *IEEE Trans. Veh. Technol.*, vol. 64, no. 11, pp. 5056–5069, Nov. 2015.
- [17] L. Guan, Z. Li, B. Hao, J. Si, and B. Ning, "Cognitive frequency hopping sequences," *Chin. J. Electron.*, vol. 25, no. 1, pp. 185–191, Jan. 2016.
- [18] L. Wei and W. Qi. (2012). "Optimization in multi-frequency interferometry ranging: Theory and experiment." [Online]. Available: <https://arxiv.org/abs/1202.1424>
- [19] D. Na and W. Zhao, *Technology of Frequency Hopping Communication Jamming and Anti-Jamming*. Beijing, China: National Defense Industry Press, 2013, pp. 76–82.
- [20] H. Zhou, C. Nicholls, T. Kunz, and H. Schwartz, "Frequency accuracy & stability dependencies of crystal oscillators," Dept. Syst. Comput. Eng., Carleton Univ., Ottawa, ON, Canada, Tech. Rep. SCE-08-12, 2008.
- [21] E. Haas, "Aeronautical channel modeling," *IEEE Trans. Veh. Technol.*, vol. 51, no. 2, pp. 254–264, Mar. 2002.
- [22] Y. Wang, L. Li, X. Ma, M. Shinotsuka, C. Chen, and X. Guan, "Dual-tone radio interferometric positioning systems using undersampling techniques," *Signal Process. Lett.*, vol. 21, no. 11, pp. 1311–1315, Nov. 2014.
- [23] Y. Wang, X. Ma, C. Chen, and X. Guan, "Designing dual-tone radio interferometric positioning systems," *IEEE Trans. Signal Process.*, vol. 63, no. 6, pp. 1351–1365, Mar. 2015.
- [24] M. Maróti *et al.*, "Radio interferometric geolocation," in *Proc. 3rd Int. Conf. Embedded Netw. Sensor Syst.*, San Diego, CA, USA, Nov. 2005, pp. 1–12.
- [25] B. J. Dil and P. J. M. Havinga, "Stochastic radio interferometric positioning in the 2.4 GHz range," in *Proc. SenSys*, Seattle, WA, USA, Nov. 2011, pp. 108–120.
- [26] W. Li, X. Wang, and B. Moran, "Resolving RIPS measurement ambiguity in maximum likelihood estimation," in *Proc. 14th Int. Conf. Inf. Fusion*, Chicago, IL, USA, Jul. 2011, pp. 1–7.
- [27] D. van der Merwe, L. Grobler, and M. Ferreira, "A study of Q-range ambiguity in the radio interferometric positioning system," in *Proc. 18th Int. Conf. Telecommun.*, Ayia Napa, Cyprus, May 2011, pp. 412–415.
- [28] D. C. Rife and R. R. Boorstyn, "Multiple tone parameter estimation from discrete-time observations," *Bell Syst. Tech. J.*, vol. 55, no. 9, pp. 1389–1410, Nov. 1976.
- [29] B. D. Rao and K. V. S. Hari, "Performance analysis of root-music," *IEEE Trans. Acoust., Speech, Signal Process.*, vol. 37, no. 12, pp. 1939–1949, Dec. 1989.
- [30] S. Tretter, "Estimating the frequency of a noisy sinusoid by linear regression (Corresp.)," *IEEE Trans. Inf. Theory*, vol. 31, no. 6, pp. 832–835, Nov. 1985.
- [31] B. Xu, W. Qi, L. Wei, and S. Zhang, "Efficient range estimation in beat radio interferometry," *IEEE Access*, vol. 5, pp. 3834–3840, 2017.
- [32] J. A. Gansman, J. V. Krogmeier, and M. P. Fitz, "Single frequency estimation with non-uniform sampling," in *Proc. Conf. Rec. 13th Asilomar Conf. Signals, Syst. Comput.*, Pacific Grove, CA, USA, Nov. 1996, pp. 399–403.
- [33] Y. V. Zakharov and T. C. Tozer, "Frequency estimator with dichotomous search of periodogram peak," *Electron. Lett.*, vol. 35, no. 19, pp. 1608–1609, Sep. 1999.
- [34] H. Messer, "The hybrid Cramer-Rao lower bound—From practice to theory," in *Proc. 4th IEEE Workshop Sensor Array Multichannel Process.*, Waltham, MA, USA, Jul. 2006, pp. 304–307.
- [35] Y. Fujiang, *Communication Anti-Jamming Engineering and Practice*. Beijing, China: Publishing House of Electronics Industry, 2008, pp. 414–419.

EN YUAN received the B.E. and M.E. degrees in computer science and technology from the PLA University of Science and Technology, Nanjing, China, in 2005 and 2008, respectively. He is currently pursuing the Ph.D. degree in computer science and technology with Army Engineering University, Nanjing. His research interests include the computer network, Internet of Things, and radio navigation.

WANGDONG QI (M'97) received the Ph.D. degree in computer engineering from the Institute of Communication Engineering, Nanjing, China, in 1997. He is currently a Professor of computer engineering with Army Engineering University. His research interests include wireless networking and radio positioning and navigation. He served on the technical program committees of numerous conferences, including the IEEE INFOCOM and the IEEE ICC.

PENG LIU received the B.E. and M.E. degrees in computer science and technology from the PLA University of Science and Technology, Nanjing, China, in 2004 and 2007, respectively. He is currently pursuing the Ph.D. degree in communication and information system with Army Engineering University. His research interests include networking and positioning in wireless networks and radio geo-location and navigation.

LI WEI received the Ph.D. degree in electronic engineering from the Institute of Communication Engineering, Nanjing, China, in 2007. He has authored or co-authored electronics letters, optimization letters, and signal processing in his research fields. His research interests include signal processing in OFDM system, Wi-Fi radar, and radio localization.

LONGLIANG CHEN received the B.E. and M.E. degrees in computer science and technology from the PLA University of Science and Technology, Nanjing, China, in 2013 and 2016, respectively, where he is currently pursuing the Ph.D. degree in computer science and technology. His research interests include wireless networking, positioning in wireless sensor networks, and indoor localization.

• • •